Self-assembled micellar nanocomplexes comprising green tea catechin derivatives and protein drugs for cancer therapy

Published in final edited form as:
Nat Nanotechnol. 2014 November ; 9(11): 907–912. doi:10.1038/nnano.2014.208.

Self-assembled micellar nanocomplexes comprising green tea catechin derivatives and protein drugs for cancer therapy

Joo Eun Chung[#1,*], **Susi Tan**[#1], **Shu Jun Gao**[1], **Nunnarpas Yongvongsoontorn**[1], **Soon Hee Kim**[2], **Jeong Heon Lee**[2], **Hak Soo Choi**[2], **Hirohisa Yano**[1,3], **Lang Zhuo**[1], **Motoichi Kurisawa**[1,*], and **Jackie Y. Ying**[1]

[1]Institute of Bioengineering and Nanotechnology, 31 Biopolis Way, The Nanos, 138669 Singapore

[2]Division of Hematology/Oncology, Department of Medicine, Beth Israel Deaconess Medical Center and Harvard Medical School, 330 Brookline Avenue, Boston, MA 02215 USA

[3]Department of Pathology, Kurume University School of Medicine, Kurume University, 67 Asahi-machi, 830-0011 Kurume, Japan

[#] These authors contributed equally to this work.

Abstract

In designing drug carriers, the drug-to-carrier ratio is an important consideration because using high quantities of carriers can cause toxicity resulting from poor metabolism and elimination of the carriers[1]. However, these issues would be of less concern if both the drug and carrier possess therapeutic effects. (-)-Epigallocatechin-3-*O*-gallate (EGCG), which is a major ingredient of green tea, has been shown to possess anticancer effects[2-7], anti-HIV effects[8], neuroprotective effects[9], DNA-protective effects[10], etc. Here we show that sequential self-assembly of the EGCG derivative with anticancer proteins forms stable micellar nanocomplexes (MNCs), which have greater anticancer effects *in vitro* and *in vivo* than the free protein. The MNC is obtained by complexation of oligomerized EGCG with the anticancer protein, Herceptin, to form the core, followed by complexation of poly(ethylene glycol)-EGCG to form the shell. When injected into mice, the Herceptin-loaded MNC showed better tumour selectivity and growth reduction, and longer blood-half-life than free Herceptin.

Many macromolecular drug carriers have been significantly improved to alter the pharmacokinetics and biodistribution of drugs[11-23], wherein the carrier is just an excipient for drug delivery and the therapeutically relevant compound is just the drug. We were inspired to design an improved delivery system whereby the carrier would display therapeutic effects. This was achieved by utilizing the binding property of EGCG with

[*]Correspondence and requests for materials should be addressed to J.E.C. and M.K. jechung@ibn.a-star.edu.sg; mkurisawa@ibn.a-star.edu.sg.

Author contributions J.E.C. and M.K. conceived and designed the experiments. J.E.C., S.T., N.Y. and S.J.G. performed the experiments. S.H.K., J.H.L. and H.S.C. performed experiments and analysed data for biodistribution and pharmacokinetic. H.Y. provided HAK-1B cells. J.E.C. and M.K. reviewed, analysed and interpreted the data. J.E.C., S.T., H.S.C., M.K and J.Y.Y wrote the paper. All authors discussed the results. J.E.C. and M.K. supervised the project.

Competing financial interests The authors declare that they have no competing financial interests.

various biological molecules including proteins[24, 25]. We synthesized a MNC carrier comprised of two EGCG derivatives designed to bind with proteins in a spatially ordered structure. One of them was oligomerized EGCG (OEGCG), which was designed to stabilize the core by strengthening the binding property of EGCG with protein[26]. The other derivative was poly(ethylene glycol)-EGCG (PEG-EGCG), which was tailored to bind with the protein/OEGCG complex as an inert and hydrophilic shell with extended PEG chains. The MNC was formed through two sequential self-assemblies in an aqueous solution: (i) the complexation between OEGCG and proteins to form the core, and (ii) the complexation of PEG-EGCG surrounding the pre-formed core to form the shell (Fig. 1a). The micellar structure with PEG shell could reduce protein immunogenicity, and prevent rapid renal clearance and proteolysis of protein, decreasing the need for frequent injections or infusion therapy[16, 21]. Although many studies have discussed the beneficial bioactivities of EGCG, in this work, we attempted to utilize EGCG as a carrier for biological molecules, aiming at combinational therapeutic effects between the carrier and the drug.

OEGCG and PEG-EGCG were synthesized by Baeyer reaction between an aldehyde group and a nucleophilic A ring of EGCG[27] (Supplementary Information, Figs. S1, S2 and S3). PEG-EGCG and OEGCG showed no and low cytotoxicity, respectively, on a human normal mammary epithelial cells (HMECs) in the range of concentrations tested, whereas they showed substantial cancer cell growth inhibitory effects on a HER2-overexpressing human breast cancer cell line (BT-474) in a concentration-dependent manner (Supplementary Information, Fig. S4).

Figures 1b and c show the transmission electron microscopy (TEM) images and the hydrodynamic diameters (HDs) of the complexes formed at each step of the two sequential self-assemblies, respectively. Herceptin (trastuzumab), which is a humanized monoclonal antibody against the HER2/neu (erbB2) receptor and induces regression of HER2-overexpressing metastatic breast cancer tumours, has a HD of ~ 9 nm. Adding OEGCG to the Herceptin solution led to the spontaneous formation of a complex with a relatively broad size distribution. TEM image of the Herceptin/OEGCG complex showed a various degree of complex association. The subsequent addition of PEG-EGCG to the Herceptin/OEGCG complexes led to the formation of monodispersed spherical complexes (~ 90 nm in HD).

The complexation of OEGCG and Herceptin was explored by dynamic light scattering by varying the concentration of each component (Fig. 2a). The size of the complex formed increased with increasing OEGCG concentrations at a constant protein concentration. However, as the Herceptin concentration increased at a constant OEGCG concentration, the complex size increased up to a maximum, followed by a decrease with further increase in Herceptin concentration. This indicated that OEGCG complexed with Herceptin via non-covalent bonds. To investigate the interaction in this complexation, Tween 20, Triton X-100, sodium dodecyl sulfate (SDS), urea and NaCl were added to the complex (Fig. 2b). Complexes were effectively dissociated by Tween 20, Triton X-100 and SDS due to hydrophobic competition. In contrast, urea (which has the ability to participate in the formation of strong hydrogen bonds and is not intrinsically hydrophobic) and NaCl were ineffective in dissociating the complexes. These results illustrated that the dominant mode of

interaction between OEGCG and proteins was hydrophobic interaction, rather than hydrogen bonding or ionic interaction.

We also studied the activities of proteins during the complexation and dissociation process. Ideally, the complexes should stably preserve the proteins from activity loss, degradation and interaction with other molecules during delivery, but exert their therapeutic activities at the sites of delivery. Figure 2c demonstrates that the activities of various proteins were restrained by the complexation with OEGCG. However, the activities were fully restored when the complexes were dissociated. The complexation of proteins could protect the proteins from potential environmental damages and undesirable side effects during delivery. Their temporarily masked bioactivity could be re-established with the dissociation of complexes when delivered/accumulated.

In order to construct the outer shell surrounding the core complex, PEG-EGCG was added to the pre-formed Herceptin/OEGCG complexes. When PEG-EGCG was added in increasing amounts to the Herceptin/OEGCG complexes of varied sizes, complexes were formed with a uniform size that remained constant, despite further increase in the PEG-EGCG concentration (Fig. 3a). TEM images showed that at increasing OEGCG concentration, the increase in the average size of Herceptin/OEGCG complex is due to increasing numbers of pre-existing Herceptin/OEGCG complexes that are complexing with each other, rather than an increase in the diameter of the pre-existing complexes (Supplementary Information, Fig. S5). This phenomenon has been known in the mechanism for polyphenol/protein complexation that the pre-existing complexes are associated by bridging through polyphenols, when the polyphenol concentration is increased[28]. The inter-complex association between Herceptin/OEGCG complexes was likely dissociated by PEG-EGCG due to hydrophobic competition with the EGCG moieties of PEG-EGCG. Subsequently, PEG-EGCG assembled around the Herceptin/OEGCG complex at the critical PEG-EGCG concentration required, yielding uniformly sized complexes under favourably balanced interaction energy. The constant complex size above the critical PEG-EGCG concentration could be due to repulsion against further assembly by the PEG outer shell that was formed.

We also found that both the composition and the sequence of addition affected the construction of the MNC (Fig. 3b). In the absence of OEGCG, PEG-EGCG still formed MNC with Herceptin, whereas PEG did not assemble with Herceptin. However, the Herceptin/PEG-EGCG complex was dissociated by the post-addition of Herceptin. In contrast, the MNC formed by the sequential two-step self-assemblies, i.e. the assembly of OEGCG with Herceptin, followed by the PEG-EGCG assembly around the Herceptin/OEGCG complex, showed no change in size despite the post-addition of Herceptin. OEGCG might have played an important role in stabilizing the complex structure by producing a more cross-linked and hydrophobic core that strengthened binding with PEG-EGCG, and the stably formed PEG shell isolated the core from the access of proteins that were subsequently added. When PEG-EGCG was added directly to OEGCG without the precomplexation of OEGCG and Herceptin, huge complexes were obtained and the size further increased with the post-addition of Herceptin. The PEG-EGCG and OEGCG were considered to form a complex by hydrogen bonding between oxygen through an ether linkage of the PEG chain and the phenolic hydroxyl group of the OEGCG[29], which was not

reversible with the post-addition of Herceptin. Therefore, pre-complexation of Herceptin/OEGCG (wherein OEGCG chains were considered to be mostly folded) was necessary to construct the stable and spatially ordered MNC. This micellar structure was supported by ζ potential study as well, which showed a significant decrease in the surface charge of Herceptin/OEGCG complex after adding PEG-EGCG, suggesting that the PEG chains covered the core complex surface (Supplementary Information, Fig. S6).

The MNC retained its integrity and confirmed good stability in the presence of serum without size change at 37°C for 15 days (Supplementary Information, Fig. S7). Also, it did not undergo any size reduction upon a thousand-fold dilution, showing excellent stability as a function of suspension dilution, which would occur *in vivo* (Supplementary Information, Fig. S8). Moreover, the fluorescence-labeled protein-loaded MNC showed a much slower increase in the fluorescence intensity, which resulted from degradation of the fluorescence-labeled protein in the presence of protease, as compared to a free protein. It demonstrated that the protein was safely protected from proteolysis by this MNC system (Supplementary Information, Fig. S9).

The anticancer effect of the Herceptin-loaded MNC was explored *in vitro* and *in vivo* and compared to that of free Herceptin (Fig. 4). The cancer cell growth inhibitory effect was observed on BT-474 (HER2-overexpressing human breast cancer cell line) after treatment with free Herceptin, Herceptin-loaded micellar nanocomplex (Herceptin-MNC), BSA-loaded micellar nanocomplex (BSA-MNC) (i.e. drug-free carrier), a mixture of BSA-MNC and Herceptin, and an equivalent amount of each carrier component (OEGCG and PEG-EGCG) (Fig. 4a). BSA-MNC showed cancer cell growth inhibitory effect due to the anticancer effect of OEGCG and PEG-EGCG; whereas BSA showed no effect. Notably, Herceptin-MNC showed a higher inhibitory effect than free Herceptin via synergism of the inhibitory effects of the carrier and Herceptin (with a combination index (CI) of 0.93) (Supplementary Information, Section 10). The greater inhibitory effect of Herceptin-MNC was also observed on other HER2-overexpressing human cancer cells (SKBR-3 and SKOV-3), whereas no growth inhibitory effect was shown on normal cells (MCF-10A and HMEC) (Supplementary Information, Fig. S10). Since the MNC was formed via hydrophobic interaction and would be dissociated by hydrophobic competition with surfactants, it could gradually dissociate and release components by interaction with bio-amphiphilic molecules, e.g. lipids of cell membrane, when they were retained with cells.

Besides Herceptin, interferon α-2a was loaded in MNC (IFN-MNC) to illustrate the *in vitro* anticancer effect of the green tea-based carrier loaded with another therapeutic protein. IFN is used in combination with chemotherapy and radiation as a cancer treatment. It has been reported to inhibit the proliferation and induce apoptosis of cancer cells in hepatocellular carcinoma[30]. IFN-MNC also showed a higher cancer cell growth inhibitory effect than free IFN on HAK-1B (human liver cancer cell line) due to synergism of the inhibitory effects of the carrier and IFN (CI = 0.46, Supplementary Information, Fig. S11a).

In Fig. 4b, the anticancer effect of Herceptin-MNC was investigated, and compared to that of free Herceptin, BSA-MNC (i.e. drug-free carrier) and sequentially injected BSA-MNC and Herceptin using a BT-474-xenografted nude mouse model (Athymic Nude-Foxn1nu,

female). The tumour treated with phosphate buffered saline (PBS) (vehicle control) progressed rapidly over 35 days. In contrast, Herceptin-MNC efficiently retarded tumour growth. Herceptin-MNC showed a significantly higher anticancer effect than sequentially injected BSA-MNC and Herceptin, as well as free Herceptin. During the period of treatment, there was no significant difference in the body weight and the survival rate between groups (Supplementary Information, Fig. S12). The mice did not show signs of toxicity (tachypnea/dyspnea, lethargy, diarrhea and abnormality in activity) and pathological changes of organs (Supplementary Information, Table S1). The results demonstrated the significant benefit of utilizing Herceptin-MNC in the BT-474 model, which could be attributed to the effects of combining Herceptin and the green tea-based MNC.

IFN-MNC also showed greatly enhanced anticancer effect on HAK-1B-xenograftednude mouse model (CrTac:NCr-Foxn1nu, female), as compared to free IFN, BSA-MNC (i.e. drug-free carrier), and sequentially injected BSA-MNC and IFN (Supplementary Information, Fig. S11b), with no significant difference in the body weight and the survival rate between groups (Supplementary Information, Fig. S13).

To assess the effectiveness of Herceptin delivery, biodistributions of Herceptin-MNC and free Herceptin in normal organs and tumour were examined (Figs. 4c and d). Heptamethine near-infrared (NIR) fluorophore ZW800-1[31] was conjugated to Herceptin for this study (Supplementary Information, Fig. S14). Herceptin-MNC exhibited 2.3-fold higher accumulation in tumour (8.4% injected dose/g organ, % ID/g), and 0.3-fold (2.1% ID/g), 0.3-fold (1.7% ID/g) and 0.6-fold (1.4% ID/g) lower accumulation in liver, kidney and lung, respectively, as compared to free Herceptin (3.7, 6.8, 6.0 and 2.4% ID/g, respectively) at 24 h post-injection. Herceptin-MNC showed over 29-fold longer blood half-life and significantly better tumour selectivity than free Herceptin (Fig. 4e and Supplementary Information, Fig. S15). Similarly, when compared with free IFN, IFN-MNC exhibited 3.2-fold higher accumulation in tumour (Supplementary Information, Fig. S11c and d), and higher selectivity and longer blood half-life (Supplementary Information, Figs. S17 and S18). These results demonstrated that protein-MNC was capable of delivering a substantially higher quantity of proteins into tumour with high selectivity and a prolonged period of blood circulation, as compared to free proteins. The intratumoural microdistribution of Herceptin-MNC was examined to study extravasation and penetration of Herceptin-MNC in tumour (Fig. 4f). Herceptin-MNCs were distributed throughout the extravascular space at 24 h post-injection, which was consistent with the localization of HER2/neu receptors overexpressed on the tumour, suggesting extravasation and deep tumour penetration of Herceptin-MNC.

We have developed and characterized the green tea-based MNC for a protein delivery whereby the carrier itself displayed anticancer effects. This system was formulated by simple self-assembly of the EGCG derivatives and proteins, and showed restraint and restoration of the protein activity upon complexation and dissociation, respectively. It effectively protected the proteins against many barriers from the point of administration to the delivery sites. The combined therapeutic effects of the green tea-based carrier and the protein drug showed greater anticancer effect than the free protein.

Methods

Materials characterization

The size and polydispersity of samples were evaluated by dynamic light scattering with a particle sizer (Brookhaven Instruments Co.). The size and morphology of the samples were characterized with a transmission electron microscope (FEI Tecnai G^2 F20 S-Twin, 200 kV).

Activity of xanthine oxidase, α-amylase and lysozyme

Xanthine oxidase activity was measured by determining uric acid production at 295 nm by an ultraviolet-visible spectrophotometer (Hitachi, Japan). α-Amylase activity was assayed with an activity kit (Molecular Probes, E-11954) using a fluorescence spectrophotometer (Hitachi, Japan, λ_{ex} = 505 nm and λ_{em} = 512 nm). Lysozyme activity was determined spectrophotometrically at 450 nm by the decrease in turbidity due to the cleavage of glucosidic linkages of micrococcus lysodeikticus.

Cell culture

BT-474 (HTB-30) was purchased from ATCC (USA). BT-474 was cultured in RPMI 1640 with HEPES buffer supplemented with 10% fetal bovine serum (FBS) and 100 units ml^{-1} of penicillin and streptomycin. The medium and supplements were purchased from Gibco.

Inhibitory effect in cancer cell proliferation

BT-474 cells were seeded (1×10^4 cells in RPMI 1640/well) in quintuplicate in 96-well microplates, and allowed to adhere overnight. The culture media were then replaced by the media containing the following samples: Herceptin (0.5 mg ml^{-1}), Herceptin-MNC (Herceptin/OEGCG/PEG-EGCG = 0.5/0.024/0.26 mg ml^{-1}), BSA-MNC (BSA/OEGCG/PEG-EGCG = 0.5/0.024/0.26 mg ml^{-1}), the mixture of BSA-MNC and Herceptin (with the equivalent), BSA (with the equivalent), OEGCG (with the equivalent), and PEG-EGCG (with the equivalent). The cells were incubated at 37°C in 5% CO_2. After 72 h, the culture media were replaced by the phenol red-free medium containing 10% Alamar Blue, which is a dye reduced by the cytochrome c activity of cells. Cell proliferation was determined from the dye reduction by monitoring the fluorescence intensity (λ ex = 549 nm and λ em = 587 nm) after 4 h of incubation. The synergism of the inhibitory effects of the carrier and protein was quantified by the Chou-Talalay method using the CalcuSyn software[32]. Statistical analysis was conducted using analysis of variance (ANOVA).

Anticancer effect in tumour-xenografted nude mice

Athymic Nude-Foxn1nu female mice were inoculated s.c. with 1×10^7 BT-474 cells suspended in 100 μl of PBS and 100 μl of Matrigel (BD Bioscience) at the right flank. One day prior to inoculation, 17 β-estradiol pellets (0.72 mg, 60-day release, Innovative Research of America) were implanted s.c. in each mouse using a trocar. Once the tumours reached a volume of 270 mm^3, 12 mice/group were randomly allocated for different treatment. Treatment was administered twice weekly via i.v. injection for 35 days with PBS (vehicle control), free Herceptin, BSA-MNC, a sequential administration of BSA-MNC and

Herceptin, and Herceptin-MNC, in the same formulations as those employed in the *in vitro* experiments. Tumours were measured twice weekly with a digital caliper, and the tumour volumes (mm^3) were calculated from the formula, volume = (length × $width^2$)/2[33]. The care and use of laboratory animals were performed according to the protocols approved by the Institutional Animal Care and Use Committee (IACUC) at the Biological Resource Centre (BRC) in Biopolis, Singapore. Statistical analysis was conducted using ANOVA.

Real-time intraoperative imaging

2-10 nmol of each compound was injected intravenously into BT-474-xenografted Athymic Nude-Foxn1nu mice. Animals were imaged at 24 h post-injection of Herceptin-MNC and free Herceptin using the fluorescence-assisted resection and exploration (FLARE™) real-time intraoperative imaging system. Excitation fluorescence rates for white light and 800 nm near-infrared excitation light were 20,000 lux and 10 mW cm^{-2}, respectively. The fluorescence (FL) and background (BG) intensities of a region of interest (ROI) over each organ/tissue were quantified using custom FLARE™ software. The contrast-to-background ratio (CBR) was calculated as CBR = (FL - BG)/BG. At least five animals were analysed. Statistical analysis was conducting using a one-way ANOVA, followed by Tukey's multiple comparisons test.

Immunohistochemistry and NIR fluorescence microscopy

The polyclonal rabbit anti-human HER2 primary antibody (Dako) was used for the tumour tissue biopsies, diluted 1:50 from the stock solution (10 μg ml^{-1}), and incubated at 4°C overnight. Goat anti-rabbit secondary antibody labeled with Alexa Fluor 680 (Invitrogen) was incubated for 1 h at room temperature at a protein concentration of 250 nM. Antibody conjugates were fixed in place with 2% paraformaldehyde. The slides were mounted with Fluoromount-G and covered with a coverslip for microscopy. Serial sections were stained with hematoxylin and eosin (H&E) using an autostainer (Leica). NIR fluorescence microscopy was performed on a Nikon TE300 with a 4-channel Nikon TE300. The excitation and emission filters used were 650/45 nm and 710/50 nm for Alexa 680 imaging, and 750/50 nm and 810/40 nm for NIR targeted tumour imaging, respectively.

Supplementary Material

Refer to Web version on PubMed Central for supplementary material.

Acknowledgments

This research was funded by Institute of Bioengineering and Nanotechnology (Biomedical Research Council, Agency for Science, Technology and Research, Singapore) and the National Institutes of Health: NIBIB grant #R01-EB-011523 (HSC). We thank A. Yamashita and J. P. K. Tan for their assistance with cell culture and TEM experiments, respectively.

References

1. Allen TM, Cullis PR. Drug delivery systems: entering the mainstream. Science. 2004; 303:1818–1822. [PubMed: 15031496]
2. Cao Y, Cao R. Angiogenesis inhibited by drinking tea. Nature. 1999; 398:381. [PubMed: 10201368]

3. Jankun J, Selman SH, Swiercz R, Skrzypczak-Jankun E. Why drinking green tea could prevent cancer. Nature. 1997; 387:561. [PubMed: 9177339]
4. Tachibana H, Koga K, Fujimura Y, Yamada K. A receptor for green tea polyphenol EGCG. Nat Struct Mol Biol. 2004; 11:380–381. [PubMed: 15024383]
5. Liang G, et al. Green tea catechins augment the antitumor activity of doxorubicin in an in vivo mouse model for chemoresistant liver cancer. Int J Oncol. 2010; 37:111–123. [PubMed: 20514403]
6. Garbisa S, et al. Tumor invasion: molecular shears blunted by green tea. Nat Med. 1999; 5:1216. [PubMed: 10545959]
7. Du GJ, et al. Epigallocatechin Gallate (EGCG) is the most effective cancer chemopreventive polyphenol in green tea. Nutrients. 4:1679–1691. [PubMed: 23201840]
8. Li S, Hattori T, Kodama EN. Epigallocatechin gallate inhibits the HIV reverse transcription step. Antivir Chem Chemother. 2011; 21:239–243. [PubMed: 21730371]
9. Yu J, et al. Epigallocatechin-3-gallate protects motor neurons and regulates glutamate level. FEBS Lett. 2010; 584:2921–2925. [PubMed: 20488180]
10. Morley N, et al. The green tea polyphenol (-)-epigallocatechin gallate and green tea can protect human cellular DNA from ultraviolet and visible radiation-induced damage. Photodermatol Photoimmunol Photomed. 2005; 21:15–22. [PubMed: 15634219]
11. Miyata K, Christie RJ, Kataoka K. Polymeric micelles for nano-scale drug delivery. Reactive & Functional Polymers. 2011; 71:227–234.
12. Musacchio T, Torchilin VP. Recent developments in lipid-based pharmaceutical nanocarriers. Front Biosci. 2011; 16:1388–1412.
13. Duncan R. The dawning era of polymer therapeutics. Nat Rev Drug Discov. 2003; 2:347–360. [PubMed: 12750738]
14. Hubbell JA. Materials science. Enhancing drug function. Science. 2003; 300:595–596. [PubMed: 12714733]
15. Kopecek J, Kopeckova P. HPMA copolymers: origins, early developments, present, and future. Adv Drug Deliv Rev. 2010; 62:122–149. [PubMed: 19919846]
16. Duncan R. Polymer conjugates as anticancer nanomedicines. Nat Rev Cancer. 2006; 6:688–701. [PubMed: 16900224]
17. Farokhzad OC, et al. Nanoparticle-aptamer bioconjugates: a new approach for targeting prostate cancer cells. Cancer Res. 2004; 64:7668–7672. [PubMed: 15520166]
18. Miura Y, et al. Cyclic RGD-linked polymeric micelles for targeted delivery of platinum anticancer drugs to glioblastoma through the blood-brain tumor barrier. ACS Nano. 2013; 7:8583–8592. [PubMed: 24028526]
19. Cabral H, et al. Targeted therapy of spontaneous murine pancreatic tumors by polymeric micelles prolongs survival and prevents peritoneal metastasis. Proc Natl Acad Sci U S A. 2013; 110:11397–11402. [PubMed: 23801758]
20. Wang F, et al. Selective tissue distribution and long circulation endowed by paclitaxel loaded PEGylated poly(epsilon-caprolactone-co-L-lactide) micelles leading to improved anti-tumor effects and low systematic toxicity. Int J Pharm. 2013; 456:101–112. [PubMed: 23968782]
21. Harris JM, Chess RB. Effect of pegylation on pharmaceuticals. Nat Rev Drug Discov. 2003; 2:214–221. [PubMed: 12612647]
22. Kim D, Gao ZG, Lee ES, Bae YH. In vivo evaluation of doxorubicin-loaded polymeric micelles targeting folate receptors and early endosomal pH in drug-resistant ovarian cancer. Mol Pharm. 2009; 6:1353–1362. [PubMed: 19507896]
23. Ishii T, et al. Treatment of cerebral ischemia-reperfusion injury with PEGylated liposomes encapsulating FK506. FASEB J. 2013; 27:1362–1370. [PubMed: 23241312]
24. Yang CS, Wang ZY. Tea and cancer. J Natl Cancer Inst. 1993; 85:1038–1049. [PubMed: 8515490]
25. Kuzuhara T, Sei Y, Yamaguchi K, Suganuma M, Fujiki H. DNA and RNA as new binding targets of green tea catechins. J Biol Chem. 2006; 281:17446–17456. [PubMed: 16641087]
26. Chung JE, Kurisawa M, Kim YJ, Uyama H, Kobayashi S. Amplification of antioxidant activity of catechin by polycondensation with acetaldehyde. Biomacromolecules. 2004; 5:113–118. [PubMed: 14715016]

27. Saucier C, Guerra C, Pianet I, Laguerre M, Glories Y. (+)-Catechin acetaldehyde condensation products in relation to wine-ageing. Phytochemistry. 1997; 46:229–234.

28. Jobstl E, O'Connell J, Fairclough JP, Williamson MP. Molecular model for astringency produced by polyphenol/protein interactions. Biomacromolecules. 2004; 5:942–949. [PubMed: 15132685]

29. Villalba JJ, Provenza FD. Preference for polyethylene glycol by sheep fed a quebracho tannin diet. J Anim Sci. 2001; 79:2066–2074. [PubMed: 11518214]

30. Hisaka T, et al. Interferon-alphaCon1 suppresses proliferation of liver cancer cell lines in vitro and in vivo. J Hepatol. 2004; 41:782–789. [PubMed: 15519651]

31. Choi HS, et al. Synthesis and in vivo fate of zwitterionic near-infrared fluorophores. Angew Chem Int Ed Engl. 2011; 50:6258–6263. [PubMed: 21656624]

32. Chou TC, Motzer RJ, Tong Y, Bosl GJ. Computerized quantitation of synergism and antagonism of taxol, topotecan, and cisplatin against human teratocarcinoma cell growth: a rational approach to clinical protocol design. J Natl Cancer Inst. 1994; 86:1517–1524. [PubMed: 7932806]

33. Sun J, et al. Antitumor efficacy of a novel class of non-thiol-containing peptidomimetic inhibitors of farnesyltransferase and geranylgeranyltransferase I: combination therapy with the cytotoxic agents cisplatin, Taxol, and gemcitabine. Cancer Res. 1999; 59:4919–4926. [PubMed: 10519405]

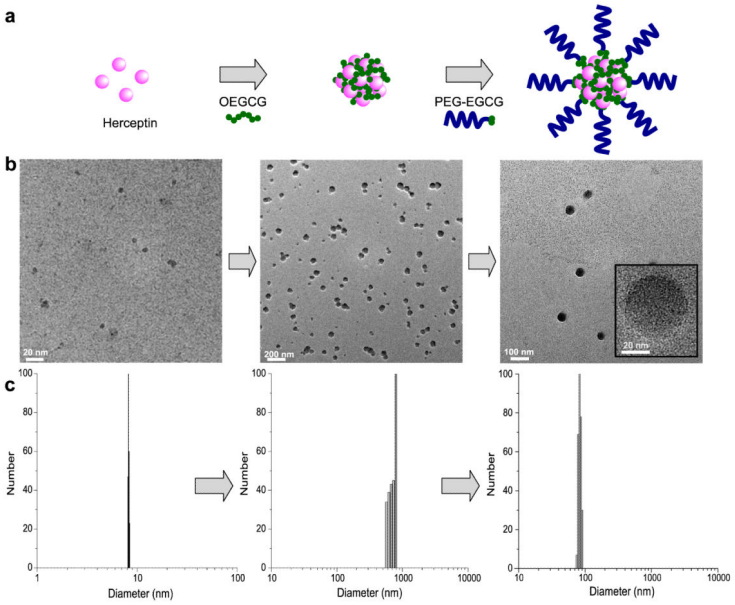

Fig. 1. Schematic diagram and morphology of self-assembled MNC loaded with proteins

a, Schematic diagram of the self-assembly process to form the MNC. The MNC was formed through two sequential self-assemblies in an aqueous solution: Complexation of OEGCG with proteins to form the core followed by complexation of PEG-EGCG surrounding the pre-formed core to form the shell. **b**, TEM images and **c**, hydrodynamic size distributions of complexes observed at each step of self-assembly.

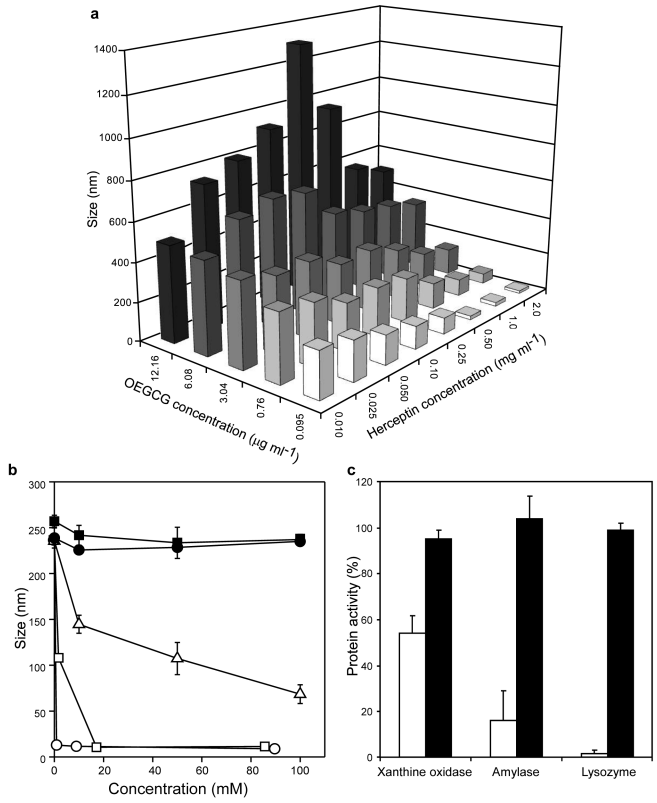

Fig. 2. Formation and dissociation of protein/OEGCG complexes

a, Size of Herceptin/OEGCG complexes formed at the given concentrations of OEGCG and Herceptin. The data indicated that OEGCG complexed with Herceptin via non-covalent bonds. The results are reported as mean values (n = 3). **b**, Complex dissociation by Tween 20 (white circles), Triton X-100 (white squares), SDS (white triangles), urea (black circles) and NaCl (black squares). Complexes were effectively dissociated by Tween 20, Triton X-100 and SDS due to hydrophobic competition, demonstrating the dominant mode of interaction between OEGCG and proteins was hydrophobic interaction. The data points represent mean values and the bars represent standard deviations (s.d.) (n = 3). **c**, Protein activities were restrained by complexation with OEGCG (white bars) and fully restored by dissociation (black bars) (protein/OEGCG w/w ratio = 1). Triton X-100 (0.1%) was used as a dissociator. The results are reported as mean values and the bars represent s.d. (n = 3).

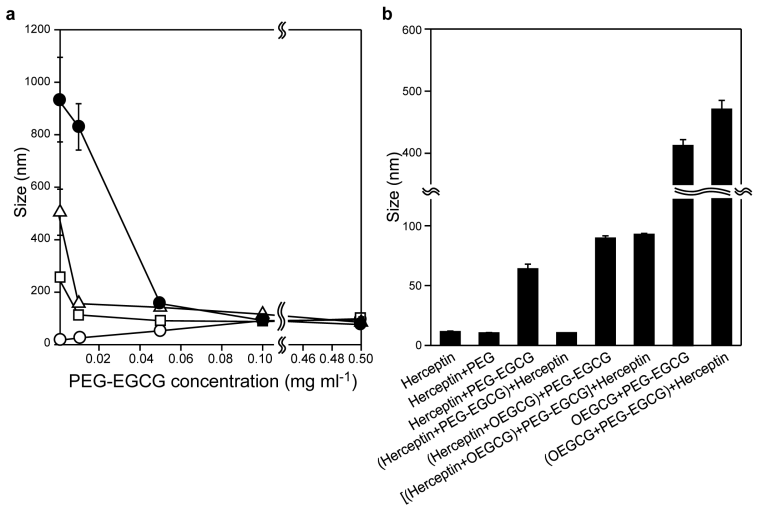

Fig. 3. The core-shell MNC formation

a, Complex size obtained when PEG-EGCG of various concentrations was added to the pre-formed Herceptin/OEGCG complexes (OEGCG = 0.09 μg ml^{-1} (white circles), 3 μg ml^{-1} (white squares), 6 μg ml^{-1} (white triangles) and 12 μg ml^{-1} (black circles)). PEG-EGCG assembled around the Herceptin/OEGCG complex of varied sizes, yielding uniformly sized complexes at the critical PEG-EGCG concentration required. The uniform size remained constant, despite further increase in the PEG-EGCG concentration. The data points represent mean values and the bars represent s.d. (n = 3). **b,** Complexes formed with various compositions and adding sequences. The sequential two-step self-assembly (the assembly of OEGCG with Herceptin followed by the PEG-EGCG assembly around the Herceptin/OEGCG complex) was necessary to construct the stable and spatially ordered MNC that showed no change in size by the post-addition of Herceptin. The results are reported as mean values and the bars represent s.d. (n = 3).

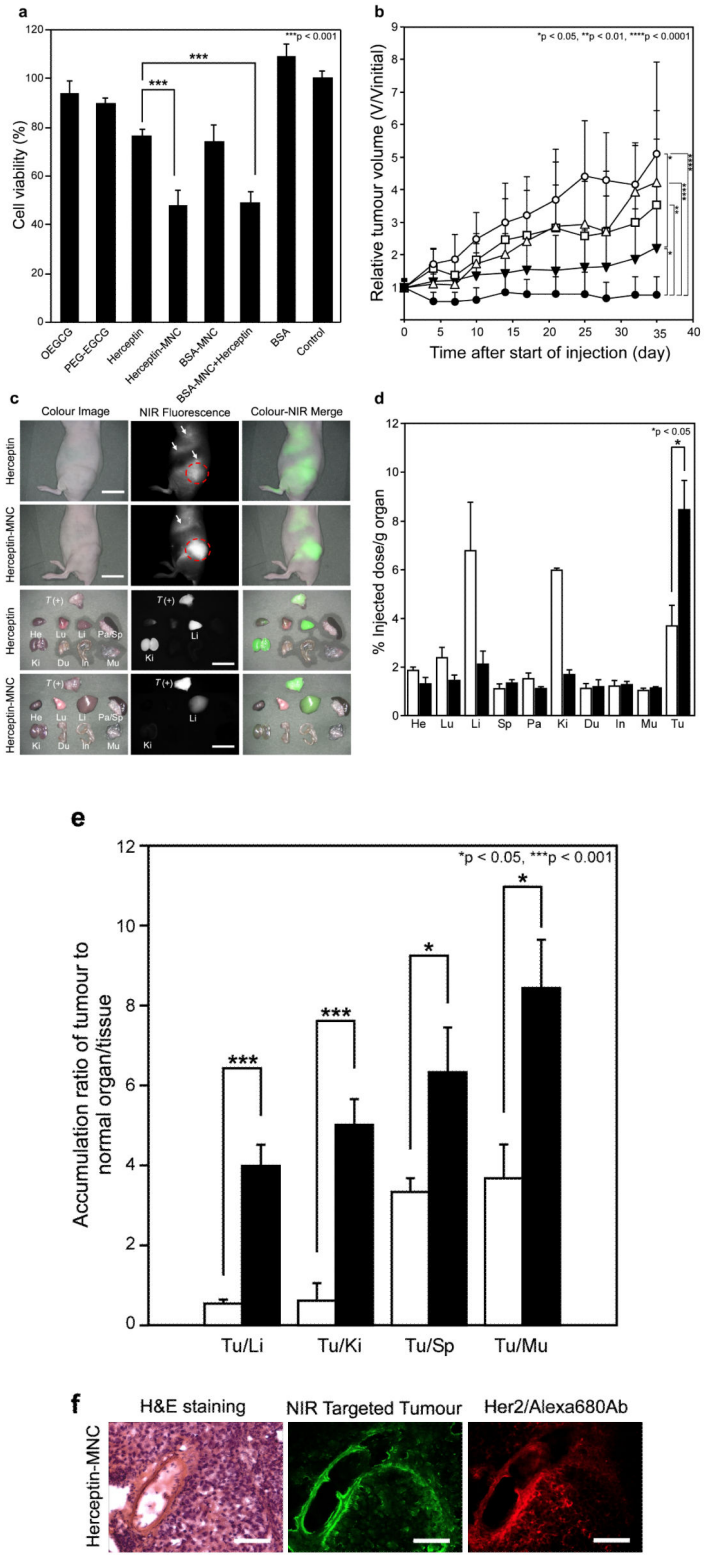

Fig. 4. The anticancer effect and biodistribution of the MNC

a, BT-474 (human breast cancer cell) growth inhibitory effects by control (untreated), Herceptin (0.5 mg ml^{-1}), Herceptin-MNC (Herceptin/OEGCG/PEG-EGCG = 0.5/0.024/0.26 mg ml^{-1}), BSA-MNC (drug-free carrier, with the equivalents), a mixture of BSA-MNC and Herceptin (with the equivalents), BSA (with the equivalent), OEGCG and PEG-EGCG (carrier components, with the equivalents). Herceptin-MNC showed a higher cancer cell growth inhibitory effect than free Herceptin via synergism of the inhibitory effects of the carrier and Herceptin. n = 5 (mean ± s.d.), ***p < 0.001. **b,** Anticancer effect on BT-474-xenografted nude mouse model. PBS (vehicle control, white circles), BSA-MNC (white triangles), Herceptin (2.5 mg kg^{-1}, white squares), sequential injection of BSA-MNC and Herceptin (black inverted triangles), and Herceptin-MNC (black circles) in the same formulations as those used in Fig. 4a. Herceptin-MNC showed a significantly higher anticancer effect than sequentially injected BSA-MNC and Herceptin, as well as free Herceptin. n = 12 (mean ± s.d.), *p < 0.05, **p < 0.01, ****p < 0.0001. **c**, Real-time intraoperative tumour detection and NIR fluorescence image-guided resection at 24 h post-injection. Arrows = nonspecific uptake (liver, kidneys, intestine); red dotted circle = ROI; *T* (+), positive tumour; He, heart; Lu, lung; Li, liver; Pa, pancreas; Sp, spleen; Ki, kidneys; Du, duodenum; In, intestine; Mu, muscle. Scale bars = 1 cm. **d,** Biodistribution of Herceptin (white bars) and Herceptin-MNC (black bars) in major organs measured at 24 h post-injection. Herceptin-MNC exhibited 2.3-fold higher accumulation in tumour and 0.3-, 0.3- and 0.6-fold lower accumulation in liver, kidney and lung, respectively, as compared to free Herceptin at 24 h post-injection. n = 5 (mean ± s.d.), *p < 0.05. **e,** Tumour-to-background (normal organ/tissue) ratio for Herceptin (white bars) and Herceptin-MNC (black bars) at 24 h post-injection. Herceptin-MNC showed the improved tumour selectivity to surrounding normal organs/tissues, as compared to free Herceptin. n = 5 (mean ± s.d.), *p < 0.05, ***p < 0.001, Tu, tumour; Li, liver; Ki, kidney; Sp, spleen; Mu, muscle. **f,** H&E staining (left), targeted NIR fluorescence (middle,pseudocoloured in lime green), and immunofluorescence staining (right, pseudocoloured in red) images of BT-474 xenograft tumour at 24 h post-injection. Herceptin-MNCs were observed throughout the extravascular space, which was consistent with the localization of overexpressed HER2/neu receptors on the tumour, suggesting extravasation and deep tumour penetration of Herceptin-MNC. Scale bars = 100 μm. All NIR fluorescence images have identical exposure times and normalization.